ACS OMEGA

Open Access

http://pubs.acs.org/journal/acsodf

Article

Systematic Engineering of Near-Infrared Small Molecules Based on 4H-Cyclopenta[1,2-b:5,4-b′]dithiophene Acceptors for Organic Solar Cells

Muzammil Hussain,[‖] Muhammad Adnan,[‖] Zobia Irshad,[‖] Riaz Hussain,[*] and Hany W. Darwish

Cite This: *ACS Omega* 2024, 9, 28791−28805

Read Online

ACCESS | Metrics & More | Article Recommendations | Supporting Information

ABSTRACT: Nonfullerene acceptors (NFAs) have emerged as tremendous materials, efficiently advancing bulk-heterojunction organic solar cells (OSCs) technology. Unlike their fullerene counterparts, NFAs offer the unique advantage of finely tunable electronic energy levels and optical characteristics, which correspond to substantial enhancement in power conversion efficiency of OSCs. Herein, we have introduced a new series of near-infrared NFAs (AY1−AY8) to advance this technology further. Our research deeply investigates the structure−property relationship and thoroughly explores the optical, optoelectronics, photophysical, and photovoltaic characteristics of a synthetic reference molecule (R) and the modeled AY1−AY8 NFAs series. We performed advanced quantum chemical simulations using density functional theory (DFT) and time-dependent DFT methods. Additionally, we also estimated key geometric characteristics such as frontier molecular orbitals, hole−electron overlap, density of states, molecular electrostatic potential, molecular excitation and binding energies, transition density matrix, and reorganizational energy of electrons and holes and compared them with those of a synthetic reference molecule (R). Our findings show that all designed materials (AY1−AY8) exhibit red-shift absorption, improved electronic charge mobility, and low binding and excitation energies compared to R. Notably, these designed materials (AY1−AY8) display significantly narrower electronic energy gaps (E_g 1.89−1.71 eV), indicating enhanced charge shifting from the highest occupied molecular orbital to lowest unoccupied molecular orbital and broadening of the absorption spectrum. Moreover, we also revealed a comprehensive study of the donor/acceptor complex of PTB7-Th/AY8 to understand charge shifting between donor and acceptor molecules. Therefore, we strongly recommend this designed (AY1−AY8) series to the experimentalists for the future development of highly efficient OSC devices.

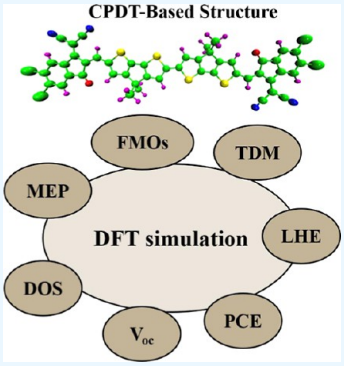

1. INTRODUCTION

Organic solar cells (OSCs) have developed rapidly during the last two decades. They are popular because they are safe, easy to make, flexible, cost-effective, and lightweight. Initially, OSCs used a material called fullerene, and they were successful for over 20 years. However, fullerenes presented several issues, including sensitivity to light, high cost, and challenges in modifying their energy level alignments. The phenomenon changed when researchers introduced nonfullerene acceptor (NFA) materials. These materials help in fixing the problems of fullerene-based materials. Then, in 2015, another breakthrough happened with the creation of fused-ring electron acceptors (FREAs). FREAs have a simple structure: an electron-rich core connected to electron-deficient parts. This structure allows them to tune different energy levels finely, absorb light, and efficiently convert sunlight into electricity. Bulk heterojunctions are crucial for solar cell devices[1−3] since they combine electron-rich and electron-deficient materials. Conjugated polymers have been used extensively as electron donors in this sector during the last several decades, whereas fullerene derivatives have been used predominantly as electron acceptors.[4] However, in recent years, nonfullerenes have emerged as a potential contender to their fullerene counterparts.[5−10] There are many benefits to using NFAs. They are lightweight and light stable, with several ways to synthesize them. Modifying the functional groups on these materials is also simple, allowing for fine-tuned control over their photoelectronic and photophysical characteristics. OSCs using electron acceptors have recently shown exceptional power conversion efficiencies (PCEs) of over 19%, thanks to recent advancements in the area. Searching for high-efficiency organic photovoltaic systems implies that electron acceptors may take over fullerenes and their properties one day. However, it is important to note that many of the high-efficiency NFAs currently in use feature large π-conjugated cores, such as indole dithiophene (IDT).[11,12] While these cores are undoubtedly effective, their synthesis poses challenges for

Received: April 3, 2024
Revised: June 6, 2024
Accepted: June 11, 2024
Published: June 19, 2024

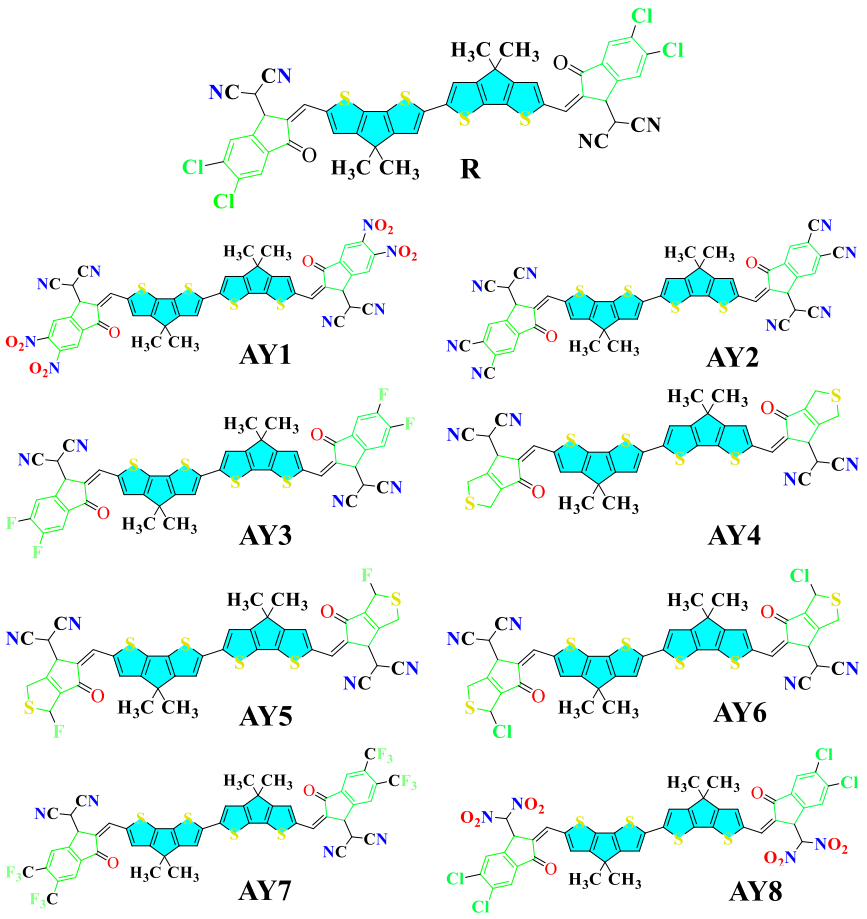

Figure 1. Molecular structures of R and newly designed molecules (AY1−AY8).

large-scale commercial applications. Consequently, there remains a pressing need in the field of OSCs for developing NFAs that deliver exceptional performance and offer straightforward and scalable synthesis routes.

The flexible electron donor unit 4Cl-cyclopenta[1,2-b:5,4-b′] dithiophene has long been used to develop organic polymers and small molecule donor materials. Because of its highest occupied molecular orbital (HOMO) level, CPDT is often used in conjunction with highly electron-deficient units like benzothiadiazole to create low-band-gap organic semiconductors.[13,14] The stiff ring-fused structures and orthogonal side chains of CPDT, IDT, and their derivatives guarantee high carrier mobility and significant solubility. These features are essential for developing solution-based techniques for producing OSCs.[29−39] Finally, this unrelenting drive demonstrates the constant shift toward more efficient and commercially viable options in electron donor and acceptor materials for bulk heterojunctions in organic photovoltaics. The change toward NFAs represents a significant leap forward, and the exploration of materials like dithiophene serves as an excellent example of the continuous efforts to simplify synthesis while maintaining or even enhancing the high performance that the field demands.

Pursuing enhanced attributes has instigated a transition from acceptors based on fullerenes to nonfullerene alternatives, which provide synthetic versatility and stability advantages. Due to their exceptional electron transport characteristics, fullerene derivatives have been widely used as electron acceptors in OSCs. NFA materials have recently been identified as a potentially effective response to these issues. These materials offer a broader range of synthetic possibilities, allowing for the fine-tuning of their electronic characteristics to optimize their performance in photovoltaic devices. Moreover, NFAs exhibit remarkable stability against environmental factors, including heat and light, which is essential for the long-term durability of solar cells. Recent breakthroughs in developing NFAs have demonstrated their potential to surpass fullerene derivatives regarding PCE. OSCs incorporating electron acceptors have shown PCEs exceeding 20%, showcasing the remarkable progress in this field. This success is paving the way for NFAs to become the new standard in organic photovoltaics.

In this study, we used synthetic reference molecules as standard molecules. Using this, we designed eight new structures by changing the end-capped acceptor groups and some electron-withdrawing groups, as shown in Figure 1.[15] We performed different analyses on these designed structures to calculate the electronic behaviors of molecules, such as transition density matrix (TDM), binding energy, excitation energy, fill factor (FF), and open-circuit voltages, and compared them to those of the reference molecule (R). Our all-designed structure has better electronic properties than R and is suitable for developing next-generation solar cell devices.

2. COMPUTATIONAL DETAILS

In this investigation, we used the programs Gauss view 5.0.8[16] and Gaussian 09[17] to perform the necessary computational analysis. To determine their absorption spectra, time-depend-

https://doi.org/10.1021/acsomega.4c03181
ACS Omega 2024, 9, 28791−28805

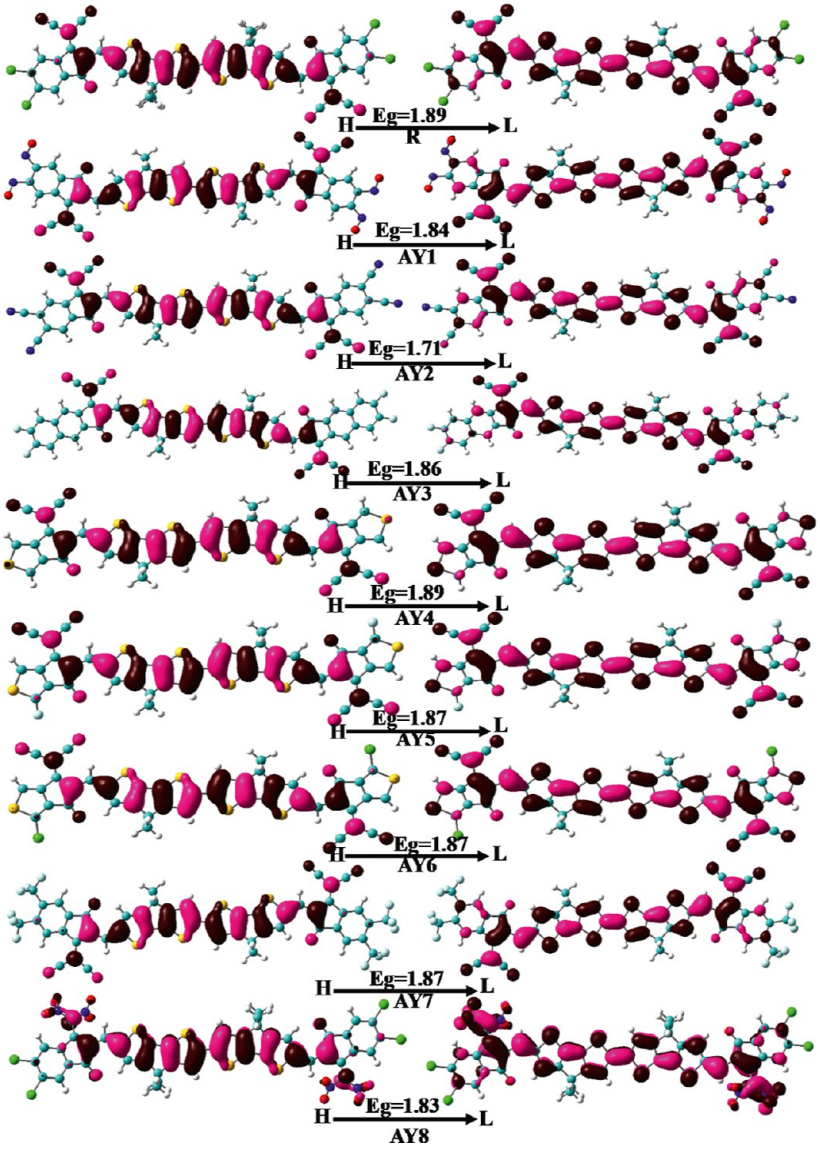

Figure 2. HOMOs and LUMOs distribution of R and the designed AY1−AY8 molecules.

ent density functional theory (TD-DFT) computations were used to visualize the reference molecule (R) and the examined structures (AY1−AY8). Absorption maxima (max) of R were calculated by TD-DFT using several functionals, such as B3LYP,[18] CAM-B3LYP,[19] MPW1PW91,[20] and WB97XD, all while employing the 6-31G (d, p) basis set. The estimated max values were compared to existing experimental data in gas and chloroform solvents to verify the DFT level that was ultimately selected. Ultimately, DFT computations were decided upon using the B3LYP technique with the 6-31G (d, p) basis set.[21] The decision was made because of its excellent agreement with experimental max values for the reference molecule (R) and all the structures (AY1−AY8) under study. These computational results were generated using the Gaussian calculations software and subsequently analyzed using software such as Origin program 8.0.[22]

Further calculations were carried out using B3LYP/6-31G (d, p) for various parameters, including the frontier molecular orbitals (FMOs) or HOMO−lowest unoccupied molecular orbital (LUMO) energy gap, charge transfer (CT) analysis for cationic, anionic, and neutral structures, and density of states (DOS) calculations for AY1−AY8 and the reference molecule. To account for solvent effects, the CPCM Model and CHCl3 solvent were employed in time-dependent self-consistent field calculations with the B3LYP/6-31G (d, p) functional to obtain UV−visible near-infrared spectra for AY1−AY8. The DOS for all the investigated compounds (AY1−AY8) and the reference molecule were calculated and analyzed using PyMOlyze 1.1[23] to assess the absorption radiation of each donor and acceptor fragment. Furthermore, TDM analysis was conducted using the Multiwfn 3.7 program package[24] to gain insights into the electronic states of excitation.

$$\lambda e = [E_0^- - E_-] + [E_0^- - E_0] \quad (1)$$

$$\lambda h = [E_0^+ - E^+] + [E_0^+ - E_0] \quad (2)$$

The following information, which stands for the necessary equations, is derived from the optimized structures: λe. The following information is required for the computation. An anion's computed energy, E_0, is the difference between the energies of a neutral atom and an anion molecule and the energy of a simple anion, E. The information needed to

https://doi.org/10.1021/acsomega.4c03181
ACS Omega 2024, 9, 28791−28805

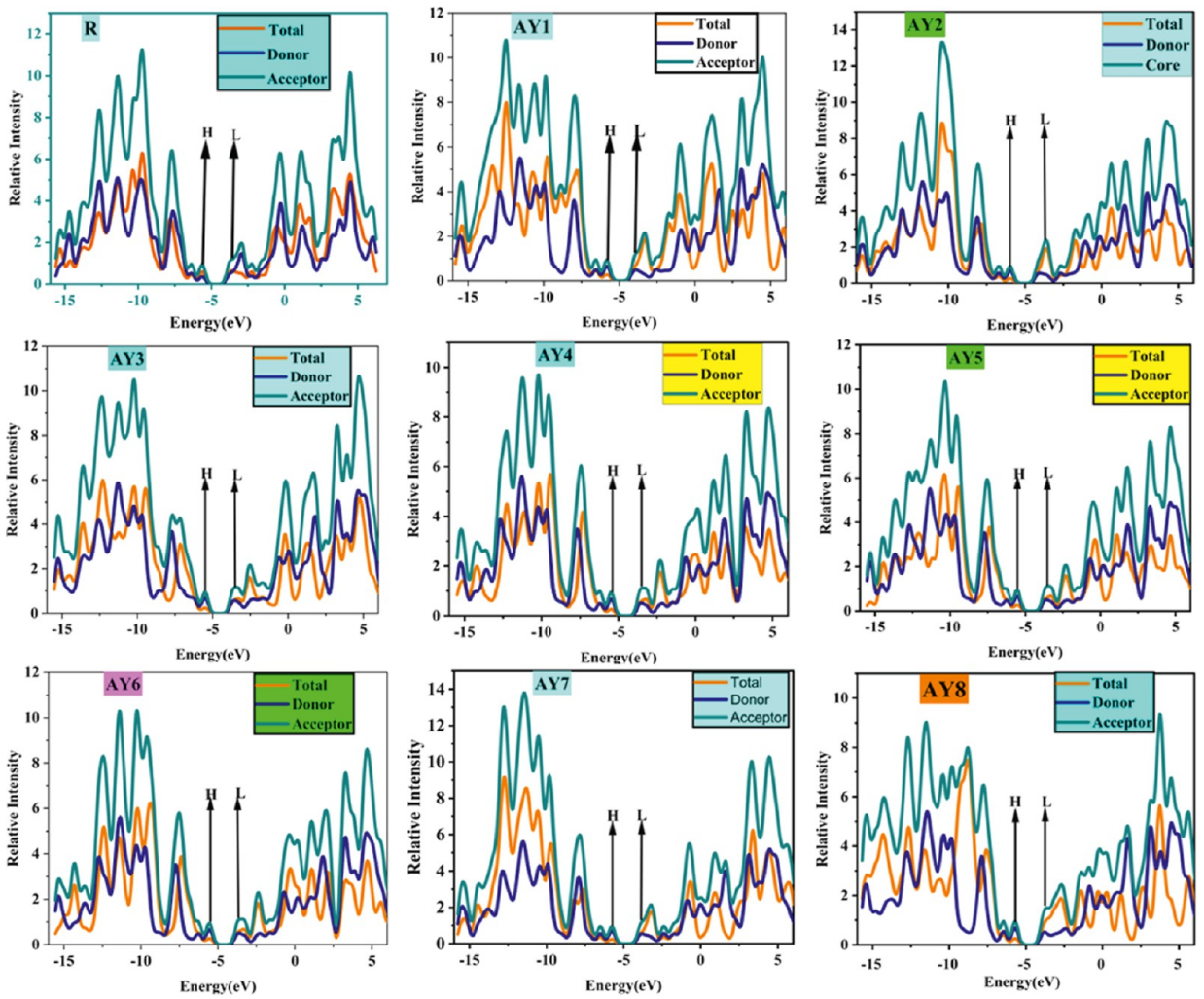

Figure 3. DOS analysis of R and the designed AY1−AY8 molecules.

determine h is as follows: E_0^+ is the energy calculated by the cation and converted to neutral, E_0^+ is the energy of the neutral molecule calculated from the optimized geometry of the cation, E^+ is the energy of a simple cation, and E_0 is the energy of neutral structures used in both eqs 1 and 2.

3. RESULTS AND DISCUSSION

3.1. Chemistry of Molecules. In our investigation, we designed different structures using different moieties and electron-withdrawing groups. We used other moieties like F, CL, NO_2, CN, and SO_3H, as represented in Figure S1 and optimized using Gaussian 09 software. The optimized structure is visualized in Figure S2 (Supporting Information).

The investigated molecules exhibit excitons that undergo a transition characterized by separating the electron and hole, with the electron transferring to the acceptor molecule and the hole remaining on the donor molecule. This type of exciton transition indicates a CT process, where the electron moves from the donor to the acceptor, signifying the potential for efficient charge separation and transport.

To verify the efficacy of this CT process, we blended acceptor molecules with the donor polymer PTB7-th. This blending strategy allows us to assess the performance of the terminal design in facilitating efficient CT at the molecular level. By evaluating the degree of CT and the resulting exciton dynamics, we gain valuable insights into the effectiveness of our terminal design for future optoelectronic applications.

Understanding and optimizing CT processes are critical for enhancing the performance of organic electronic devices, such as solar cells and light-emitting diodes. By demonstrating the CT nature of excitons and evaluating the CT efficiency in blended systems, our research lays the groundwork for developing advanced materials with improved charge transport properties. This knowledge paves the way for designing more efficient and sustainable optoelectronic devices, contributing to advancements in renewable energy and electronic technology.

3.2. Basis Set Selection. The initial step in our study involved determining the maximum wavelength (λ_{max}) of (R) in the solvent ($CHCl_3$). To accomplish this, we employed DFT calculations with six different functionals: B3LYP, ωB97XD, M06-2X, MPW1PW91, M06, and CAM-B3LYP while utilizing the 6-31G (d, p) basis set. Each of the six functionals calculated theoretical λ_{max} values for chloroform as follows: 791.98, 587.71, 746.13, 569.25, 587.25, and 569.76 nm, respectively. Note that the reference molecule's maximum wavelength (max) was measured experimentally and determined to be 776 nm (reference). Thus, the B3LYP functional approach, in combination with the basis set 6-31G(d, p), was chosen to compare these theoretical conclusions to the actual data. This option was selected because it agrees closely with

https://doi.org/10.1021/acsomega.4c03181
ACS Omega 2024, 9, 28791−28805

the experimentally observed λ_{max} value, as shown in Figure S3. This decision guarantees that our findings align with the experimental data and provide a firm basis for future studies.

3.3. Frontier Molecular Orbitals. Delving into MO theory, we explored the FMOs for the reference R and the designed AY1−AY8 molecules. FMOs, comprising the HOMO and the LUMO, as illustrated in Figure 2, hold the key to understanding and optimizing molecular optical properties.[25]

In this study, we harnessed the efficacy of the B3LYP functional, selected for its exceptional accuracy in matching λ_{max} values of synthesized reference molecules. Paired with the 6-31G (d, p) basis set, we conducted FMO calculations for all the molecules, shedding light on their intricate electronic structures. At the heart of the solar cell photovoltaic efficiency lies the HOMO − LUMO energy gap, commonly called the band gap or conduction band. This gap is the linchpin for dictating the CT speed between MOs, ultimately shaping the CT dynamics within a molecule.[26−28] Our research explores the critical role of newly designed NFAs in determining these properties, paving the way for innovations in solar cell technology that can harness the full potential of renewable energy sources.

The computed values for the HOMO and LUMO energies of the reference molecule are −5.63 and −3.74 eV, respectively. The HOMO energies of the eight newly developed molecules (AY1−AY8) are as follows: −5.83, −5.83, −5.85, −5.51, −5.54, −5.56, −5.77, and −5.70 eV, respectively. Figure 2 also displays the energy gap between the HOMO and LUMO of reference and designed molecules.

By comparing AY4 and AY3, we can see that AY4 has a lower HOMO energy value because its end-cap acceptor moieties, AY8 and AY2, are more efficient. Intriguingly, the LUMO energies of the newly designed molecules are comparable. This is likely the result of the addition of functional end-capped acceptor moieties. The reference molecule has an energy gap of 1.89 eV, whereas the developed molecules (AY1−AY8) have gaps of 1.84, 1.71, 1.86, 1.89, 1.87, 1.87, and 1.83 eV, respectively. The end-capped acceptor moieties are principally responsible for the reduced HOMO − LUMO energy gaps in all the developed compounds compared to that of the reference molecule, as tabulated in Table S1 (Supporting Information). Since its acceptor unit is end-capped, AY8 has the smallest HOMO − LUMO energy gap, at just 1.83. The energy difference between the HOMO and LUMO states of the investigated compounds may be rated as follows, from highest to lowest: after AY8, R comes in ahead of AY4, AY5, AY6, and AY7. These results demonstrate the great promise of the engineered molecules AY1−AY8 as materials for next-generation OSCs with superior photovoltaic performance.[29,30]

3.4. DOS Analysis. The B3LYP DFT functional was used to calculate the DOS at the 6-31G (d, p) level of theory. Figure 7 shows the DOS plots for the reference molecule (R) and the eight acceptor molecules (AY1−AY8). A close inspection of Figure 3 reveals that the electron-attracting properties of the end-capped acceptor moieties have significantly altered the distribution patterns of the HOMO and LUMO charge densities.

The HOMO density is mostly dispersed over the donating core in R, the reference molecule. In contrast, the accepting region of the molecule is where the LUMO density is most concentrated. On the other hand, a noticeable change in the distribution of charge densities is seen for molecules AY1−AY8, while the donor entity and the bridging section of the molecule have a disproportionate share of the molecule's HOMO density in contrast to the acceptor unit. Such a striking finding in the acquired DOS plots proves that the end-capped acceptor molecules efficiently distribute electron density.

Therefore, the DOS calculations have unveiled a profound transformation in the charge density distribution patterns, highlighting the capacity of end-capped acceptors to efficiently draw and facilitate electron movement within these molecules, which is a promising characteristic for their potential application in various electronic devices, including OSCs.[31,32] For a better insight into these terminal acceptors, we have calculated the percentage (% age) of donor and acceptor group contributions. In our reference molecule structure, the % age contribution of donor parts is higher than that of acceptor parts. After modeling new terminals, there is a larger contribution of acceptors, proving that our design is better for designing materials for next-generation organic photovoltaic applications. As per the reason, our acceptor's groups are electron-deficient, and they withdraw charge from the donor part, as provided in below mentioned Table S2.

3.5. Light Harvesting Efficiency. Light harvesting efficiency (LHE) is the ability of a solar cell to capture and convert sunlight into electrical energy effectively. It is a crucial factor in determining the overall performance of a solar cell. Assessing a compound's ability to produce charge following light absorption or to induce the conduction band is critical when evaluating its suitability in a solar cell. Equation 3 calculates the LHE.[33]

$$\mathrm{LHE} = 1 - 10^{-f} \tag{3}$$

The LHE was calculated using eq 3, where "f" represents the oscillator strength. The oscillator strength of the solvent phase is utilized to determine the LHE. The theoretically calculated LHE values for R and AY1−AY8 in the solvent and gas phases are presented in Tables S3 and S4. Notably, AY3 exhibits the highest LHE value among all the molecules, which is 0.9997. As per the equation below eq 4, LHE directly correlates with the short-circuit current (J_{sc}).[34]

$$J_{sc} = \int_{\lambda}^{0} \mathrm{LHE}(\lambda)\cdot\varphi_{inj.}\eta_{\mathrm{collect.}}\,\mathrm{d}\lambda \tag{4}$$

In the provided eq 4, LHE represents the light harvesting efficiency, J_{sc} corresponds to the short-circuit current, η_{collect} signifies the gathered charge assembly, and ϕ_{injected} stands for the electron injection. This equation establishes a direct connection between LHE and J_{sc}. Consequently, any variations in LHE directly influence J_{sc}, and both are present in the graph, as shown in Figure S4. All our designed molecules have LHEs as R > AY-3 > AY-1AY-4 > AY-5 > AY-6 > AY-7 > AY-2 > AY-8 in chloroform and AY3 > R > AY1 = AY2 > AY4 = AY5 = AY6 = AY7 > AY8 in the gas phase, as mentioned in Figure S4.

3.6. Molecular Electrostatic Potential Analysis. Molecular electrostatic potential (MEP) offers a three-dimensional visualization of how electric charge is distributed within a molecule. It serves as a guide to identifying regions within the molecule that are electron-rich or electron-poor. MEPs are depicted as colorful maps, providing insights into the presence of electron-withdrawing functional groups[35]

When examining the MEP plots of the investigated molecules, we observe that oxygen and nitrogen atoms display a significant red color, indicating a high electron density in

https://doi.org/10.1021/acsomega.4c03181
ACS Omega 2024, 9, 28791−28805

these areas (Figure 4). In addition, the fluorine atoms at the terminal acceptor groups have a faint red hue, indicating high

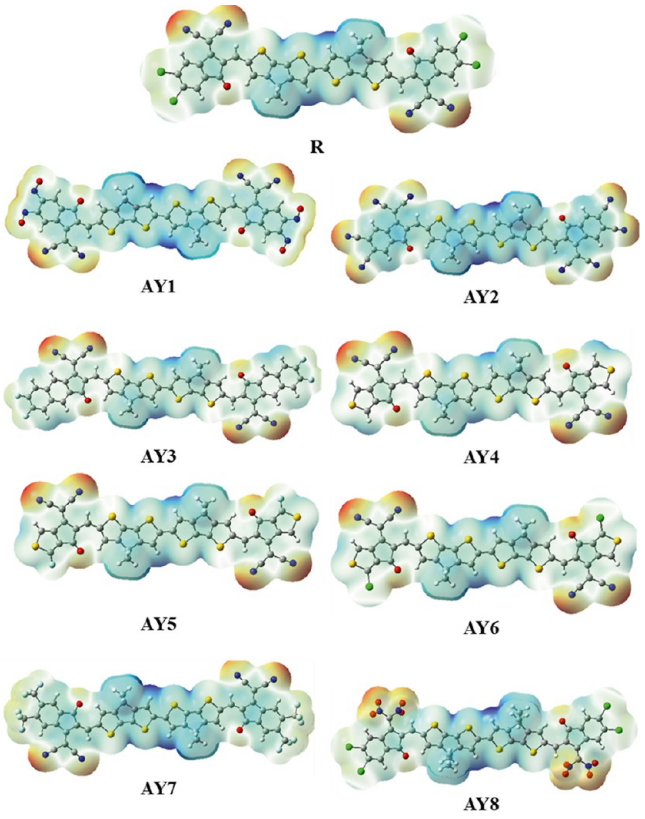

Figure 4. MEP analysis of R and the designed AY1−AY8 molecules.

electron density. On the other hand, the MEP maps show the carbon atoms in the nonfused thiophene rings in the molecules' centers to be blue. This blue hue indicates a severe lack of electrons in these atomic sites. These MEP maps provide essential information on these substances. Charge and electron distribution are visualized in Figure 4.

3.7. Transition Density Matrix. The TDM gives qualitative insights into the electronic excitations, transition dynamics, and two-dimensional motion of electrons inside conjugated molecular structures. It provides insights into how hole−electron couples function inside these molecules. This research used the theory model's 6-31G (d,p)/B3LYP level to determine TDM energy levels. We then used the Multiwfn_3.7 (Multiwave function) program to create graphic representations of these systems. The *x*- and *y*-axes in the diagrams show the total number of atoms in a given molecule, eliminating hydrogen atoms owing to their negligible contribution to conjugation.

The *y*-axis on the right shows the electron density coefficient values. Our examination of all the molecules we looked at, including R and AY1−AY8, shows that the electron density is spread throughout these structures, with a concentration in the donor areas, as shown in Figure 5. There is a more significant diagonal tendency from the donor to the acceptor. However, electronic consistency propagates in both directions inside the molecules. The exciton binding (E_b) energy is a valuable metric for elucidating the nature of the Coulombic charges that develop between charge carriers in conjugated molecules due to photoexcitation. The Coulombic interactions between electron−hole pairs are less in molecules with lower binding energies, allowing them to migrate more quickly away from the molecules and toward the electrodes. The calculation of E_b was carried out using eq 5.[36]

$$E_b = E_g - E_{opt} \tag{5}$$

In eq 5, E_g represents the energy gap, and E_{opt} represents the optical band gap of materials. The exciton and E_b values for all the molecules under investigation were determined in both gas and solvent phases, and these values are presented in Table 1.

AY2 has the lowest E_b value of all the compounds tested in the gaseous and solvent phases. Because of this property, AY2 is a good candidate for increasing current charge density since its excitons quickly disperse into free charge carriers. It is worth noting that polar solvents have a pronounced effect on excitons, leading to solid interactions and bonding. Consequently, E_b tends to have a higher value in solvents like chloroform than in the gaseous phase.

3.8. Optoelectronic Properties. The UV−visible analysis in chloroform and the vacuum phase was conducted through DFT calculations, as shown in Figure 6. The 6-31G (d,p)/B3LYP level of theory was employed to determine various features such as (λ_{max}), (f), (E_x), and electron transport percentage (% age) in $CHCl_3$, as detailed in Table 2.

The absorption spectrum was determined using TD-DFT computations at the 6-31G (d,p)/B3LYP level for chloroform solvent and the gas phase. Table S5 provides the computed excitation energy (E_x), maximum absorption wavelength (λ_{max}), and oscillator strength (f) in the gas phase. The gas phase λ_{max} values for the suggested compounds varied from 658 to 807 nm. Specifically, the determined λ_{max} values for AY1, AY2, AY3, AY4, AY5, AY6, and AY7 are as follows: 815.52, 823.98, 802.49, 782.28, 788.85, 792.74, 796.92, and 845.39 nm, respectively. Notably, AY2 exhibits the highest λ_{max} value compared to the reference molecule owing to the extended conjugation of the end-capped group. These results show that a red absorption spectrum shift occurs when the conjugation time with the donor unit is extended (28).

Furthermore, AY3 has a more protracted absorption wavelength than AY5 owing to the presence of the nitro group. However, compared to the reference molecule and the other created molecules, the absorption patterns of AY6 and AY7 are similar. These results shed light on the examined compounds' maximum absorbance, excitation energies, and oscillator strengths. Among the studied molecules, AY2 stands out with the most remarkable λ_{max} value at 823.98 nm. The AY3 molecule's substantial conjugation between its acceptor end-capped moiety and donor core is responsible for its massive uptake. In contrast, AY2 has a more significant red shift than AY6 because of the −CN group's presence in the donor core. The reference chemical has a maximum wavelength of 791.98 nm, worth mentioning.

In the solvent phase, the oscillator strength () values are relatively higher than in the gas phase. This suggests that the solvent phase may be more favorable for blend formation, potentially enhancing the probability of photon absorption and thereby improving the photophysical characteristics of the materials. In other words, higher f values directly correlate with the absorption phenomenon in materials, making it desirable to achieve high values for organic semiconducting materials. In this context, all the designed materials demonstrate good and comparable f values in both solvent and gas-phase media,

https://doi.org/10.1021/acsomega.4c03181
ACS Omega 2024, 9, 28791−28805

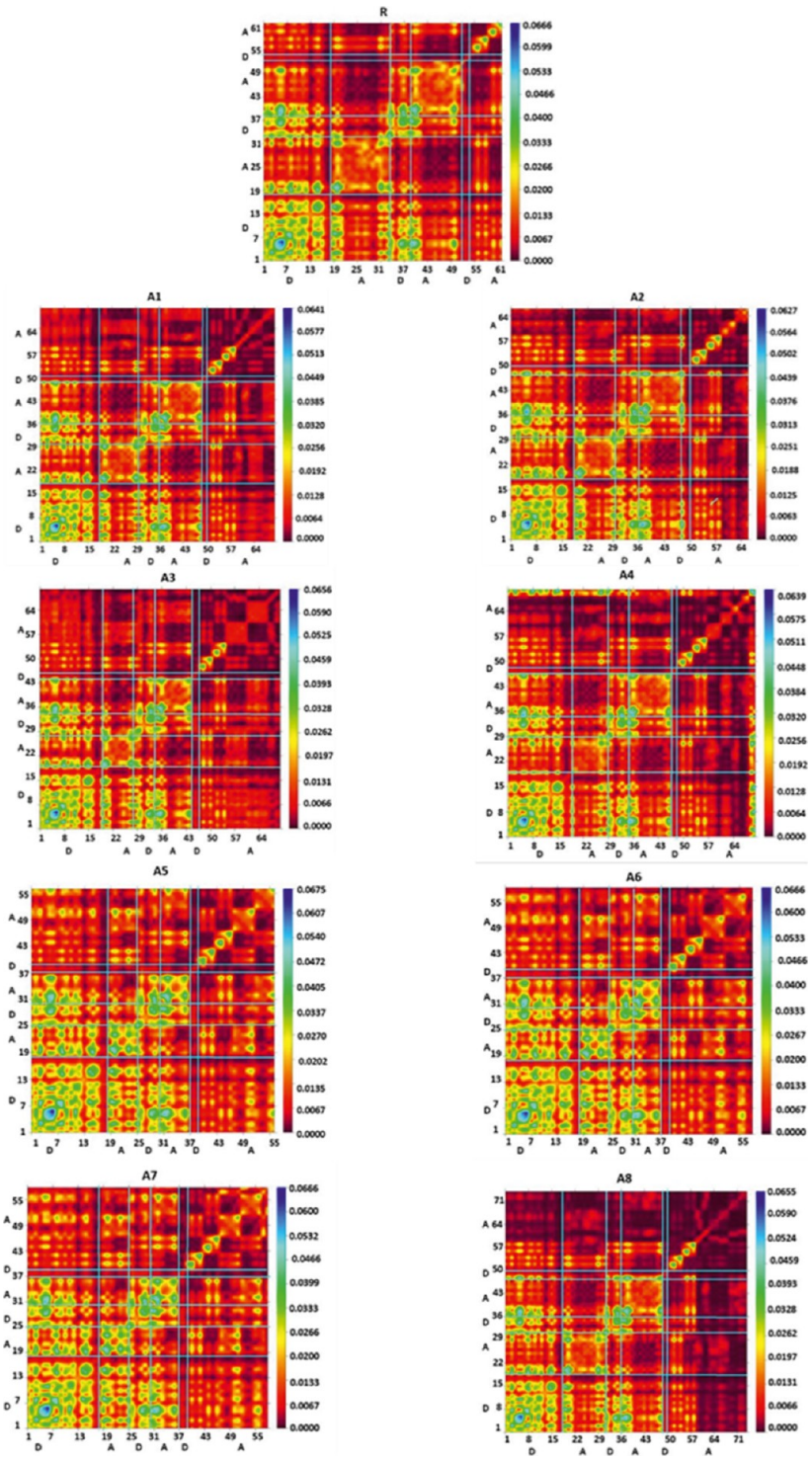

Figure 5. TDM analysis of R and the designed AY1−AY8 molecules.

highlighting the effectiveness of our design strategy in creating strong photovoltaic materials.

The efficiency of OSCs can also be assessed using excitation energy, where low excitation energy values are often associated with high OSC efficiency. Low excitation energy facilitates the allocation of electron density from the HOMO to the LUMO. In both the $CHCl_3$ and gas phases, the E_x values for all molecules were examined, and they consistently exhibited low excitation energy and strong oscillation strength. Specifically, the excitation energies for the proposed molecules (AY1−AY8) in $CHCl_3$ ranged from 1.74 to 1.66 eV, while in the gas phase, they ranged from 3.54 to 2.91 eV. These comparable excitation energy values indicate that these molecules are promising candidates for more efficient OSCs. Furthermore, the orbital assignments are highly significant, with over 99% agreement in solvent and gas phases. For OSCs to exhibit excellent performance, maximum transitions between orbitals should occur in both stages, which is desirable.

3.9. Heat Mapping Analysis. Through a thorough theoretical analysis, the investigation delved into the intriguing

https://doi.org/10.1021/acsomega.4c03181
ACS Omega 2024, 9, 28791−28805

Table 1. Energy Gap and First Singlet Excitation Energy and Binding Energy

molecules	E(H−L) (eV)	E_{opt} (eV)	$E_b = E_g - E_{opt}$ (eV)
R	1.89	1.74	0.15
AY-1	1.84	1.70	0.14
AY-2	1.71	1.69	0.02
AY-3	1.86	1.71	0.15
AY-4	1.89	1.75	0.14
AY-5	1.87	1.74	0.13
AY-6	1.87	1.73	0.14
AY-7	1.87	1.73	0.14
AY-8	1.83	1.68	0.15

realm of electron−hole interaction within molecules AY1−AY8 and the R molecule. The revealing results are elegantly depicted in Figure 7, encapsulating the essence of this interaction. A remarkable finding emerges from these graphical representations: AY1 to AY8 molecules exhibit notable intertwining between their electrons and holes. Among these molecules, AY4 shines as a standout, displaying an exceptionally intense level of overlap. This phenomenon can be ascribed to the relatively modest band gap and the impressive mobility of both electrons and holes within the molecular framework. This comprehensive exploration of electron−hole interaction, underpinned by solid theoretical underpinnings, underscores these recently crafted molecules' unique prowess and potential. They possess a distinct capability for outstanding performance, mainly when deployed as the active layer in OSCs.

In conclusion, the encouraging levels of electron−hole interaction observed in the AY1 to AY8 molecules, with AY4 as a prime example of intense overlap, position them as potential game-changers in the field of OSCs. These molecules embody the inherent qualities necessary for facilitating efficient charge transport and separation, a key factor in pursuing high-performance OSCs. This research opens up exciting possibilities for the future of OSCs, inspiring further exploration and innovation in this field.

3.10. Dihedral Angle Measurements. Certainly, in computational and theoretical chemistry, a dihedral angle, also known as a torsion angle or torsional angle, is an angular measurement that quantifies the rotation between two intersecting planes defined by sets of four atoms, each as shown in Figure 8. These angles are calculated for several vital reasons. First, they play a crucial role in understanding and predicting molecules' 3D conformation or shape, which is essential for determining their reactivity, stability, and interactions. Second, dihedral angles are vital in studying mechanisms and predicting reaction paths, especially in reactions requiring bond rotations. These angles significantly describe the structure in chemistry, affecting folding, stability, and function. In addition, they are constantly tracked in molecular dynamics simulations and are crucial in DFT calculations for correct electronic structure identification and conformational analysis. Dihedral angles are vital in our investigation because they provide information about molecule behavior and characteristics.

3.11. Quantum Chemical Parameters. Descriptors resulting from quantum mechanics computations are called quantum descriptors, QM descriptors, and other variations of these terms. The electronic structure and behavior of molecules, atoms, and materials may be better understood using these labels. They are frequently employed in computational chemistry and materials research to understand better and anticipate diverse chemical and physical events. Here, we can calculate the following equation using the following equation, and their values are tabulated in Table 3. Chemical softness and hardness play a vital role in the stability and reactivity of the reference compound and designed molecules, and their graphical representation is shown in Figure 9. Softness enhances light absorption and CT, while hardness ensures material stability. Achieving the right balance is crucial for efficient solar cell design. Softness refers to the ease with which a molecule or material can undergo electronic changes (such as CT) in response to external perturbations. Hardness is the inverse of softness. It represents the resistance of a material to electronic changes. Materials with wider band gaps (greater hardness) are more stable but may absorb light less effectively.

The E_{H-L} gap energy is determined by using eq 6.

$$E_{H-L} = E_{HOMO} - E_{LUMO} \quad (6)$$

Electron affinity (EA) is determined by using eq 7.

$$\text{Electron affinity} = \text{EA} = -E_{LUMO}\ (\text{eV}) \quad (7)$$

Ionization potential (IP) is determined by using eq 8.

$$\text{Ionization Potential} = \text{IP} = -E_{HOMO}\ (\text{eV}) \quad (8)$$

Chemical potential (μ) is determined by using eq 9.

$$\text{Chemical potential} = \mu = -\frac{(\text{IP} + \text{EA})}{2} \quad (9)$$

Chemical hardness (η) is determined by using eq 10.[36]

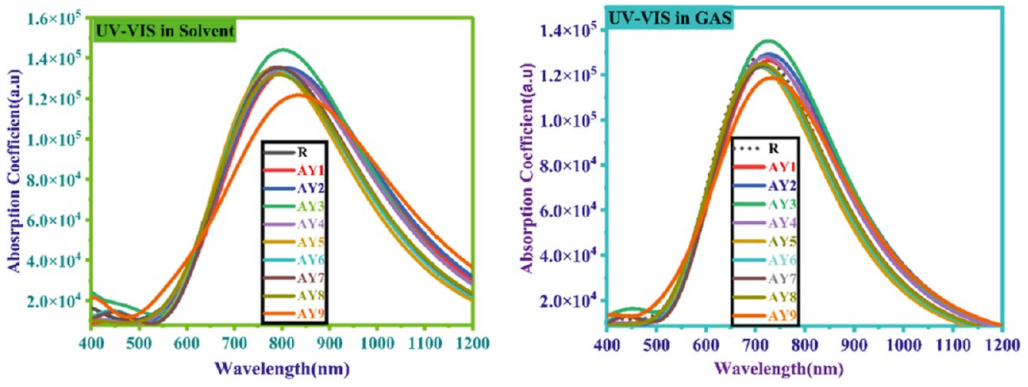

Figure 6. UV−visible absorption phenomenon of R and the designed AY1−AY8 molecules in the gas and solvent phases.

https://doi.org/10.1021/acsomega.4c03181
ACS Omega 2024, 9, 28791−28805

Table 2. λ_{max}, % Age Electron Transportation, and Oscillating Strength of R and Designed AY1−AY8 Compounds in the Solvent Phase

molecules	DFT calculated λ_{max} (nm)	experimental λ_{max} (nm)	E_x (eV)	f	major MO assignment
R	791.98	776	1.57	3.33	HOMO → LUMO (99%)
AY-1	815.52		1.52	3.26	HOMO → LUMO (99%)
AY-2	823.98		1.50	3.14	HOMO → LUMO (99%)
AY-3	802.49		1.54	3.55	HOMO → LUMO (99%)
AY4	782.28		1.58	3.33	HOMO → LUMO (99%)
AY-5	788.85		1.57	3.33	HOMO → LUMO (99%)
AY-6	792.74		1.56	3.34	HOMO → LUMO (99%)
AY-7	796.92		1.56	3.21	HOMO → LUMO (99%)
AY-8	845.39		1.47	2.91	HOMO → LUMO (99%)

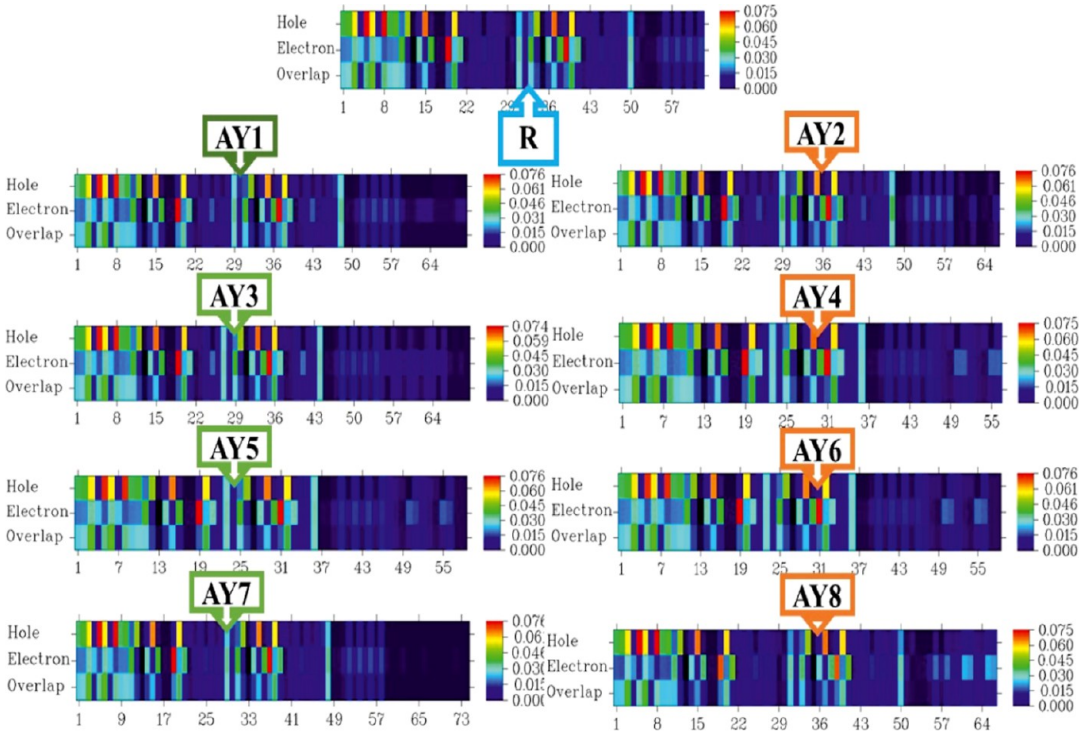

Figure 7. Heat map analysis (hole/electron overlap) of R and the designed AY1−AY8 molecules.

$$\text{Hardness} = \eta = \left(\frac{(\text{IP} - \text{EA})}{2}\right) \quad (10)$$

Chemical softness (S) is determined by using eq 11.[37]

$$\text{Chemical softness} = S = \frac{1}{2\eta} \quad (11)$$

3.12. Reorganizational Energy Analysis. The reorganization energy plays a crucial role in determining the efficiency of charge mobility in solar cells by influencing the movement of both holes and electrons when excited. This phenomenon is especially significant in evaluating the effectiveness of SCs. The CT from the donor core to the acceptor end-capped portion can be precisely calculated with proper assistance. It is worth noting that materials exhibiting strong photovoltaic effects tend to have lower reorganization energy values, a characteristic that leads to enhanced charge mobility, as depicted in Figures S6 and S7.

Two types of reorganization energy have been discovered in SC compounds: exterior reorganization energy (ext) and internal reorganization energy (int). While external factors can be controlled somewhat, this discussion will primarily focus on λint. By utilizing the Marcus equation,[38−40] we can evaluate both hole mobility (λh) and electron mobility (λe). For reference, let us compare the reorganization energy values of the molecule R and the proposed molecules AY1−AY8, specifically concerning electrons and holes. The results are tabulated in Table S6. For the R molecule, the values of λe and λh are 0.2259 and 0.4671 E_h, respectively. The electron mobility (λe) follows this sequence: AY2 > AY1 > AY8 > AY7 > R > AY6 > AY3 > AY5 > AY4. Notably, AY4, AY3, and AY6 display lower λe values than R, suggesting their suitability for electron mobility applications. When examining hole mobility (λh), the order is as follows: AY2 > AY1 > AY7 > AY8 > R > AY6 > AY5 > AY4 > AY3. This indicates that AY2, AY1, AY7, and AY8 exhibit higher hole mobility characteristics.[41−43]

Compared to R, the suggested materials have superior electron and hole mobility, as discussed in the section on reorganization energy. These values are noticeably reduced since we successfully engineered molecules with advantageous functional groups (−NO_2, −F, −Cl, and −CN).[44] The photovoltaic characteristics of the modified materials have been significantly improved. Figure 10 shows other proper

https://doi.org/10.1021/acsomega.4c03181
ACS Omega 2024, 9, 28791−28805

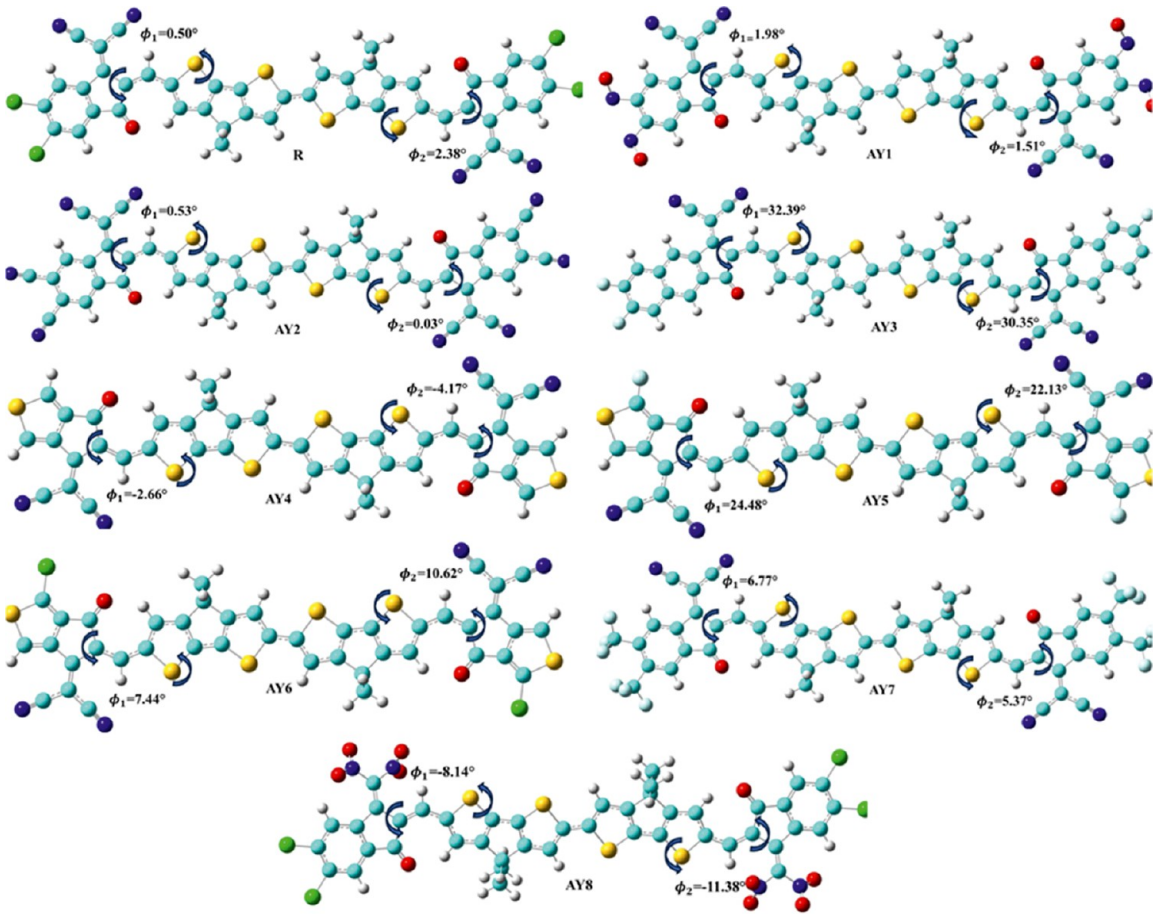

Figure 8. Dihedral angles of R and the designed AY1−AY8 molecules.

Table 3. IP, EA, Chemical Potential, Softness, Hardness, Electronegativity, and Total CT

molecules	IP	EA	μ (eV)	η (eV)	S (eV)	χ (eV)	ω (eV)	ΔNmax (e)
R	5.63	3.74	−4.69	0.94	0.53	4.69	11.64	4.97
AY-1	5.83	3.99	−4.91	0.92	0.54	4.91	13.09	5.34
AY-2	5.85	4.14	−4.99	0.85	0.59	4.99	14.61	5.85
AY-3	5.51	3.65	−4.58	0.93	0.54	4.58	11.26	4.92
AY-4	5.48	3.59	−4.54	0.94	0.53	4.54	10.89	4.80
AY-5	5.54	3.67	−4.60	0.94	0.53	4.60	11.33	4.92
AY-6	5.56	3.69	−4.62	0.93	0.54	4.62	11.44	4.95
AY-7	5.77	3.89	−4.83	0.94	0.53	4.83	12.47	5.16
AY-8	5.70	3.87	−4.79	0.92	0.55	4.79	12.52	5.23

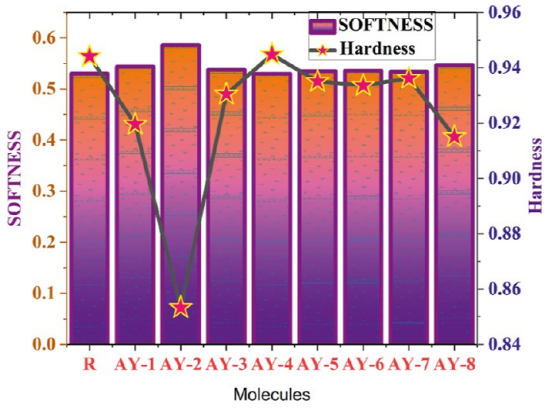

Figure 9. Softness and hardness of R and the designed AY1−AY8 molecules.

values for T_{hole} and $T_{electron}$. T_{hole} and $T_{electron}$ provide information about the time duration through which designed molecules offer CT when photovoltaic phenomenon act on the surface and then during excitation, holes and electrons are created.

The higher values of electron reorganization energy observed in NFAs than in their hole counterparts are due to several factors. First, NFAs often undergo more significant structural rearrangements upon structural modeling. These structural distortions lead to larger changes in bond lengths, bond angles, and overall molecular conformation, resulting in higher reorganization energies. Second, the electronic configurations of NFAs inherently favor larger reorganization energies due to their specific MO distributions and energy levels. Additionally, the presence of certain functional groups and substituents in NFAs contribute to increased electron

https://doi.org/10.1021/acsomega.4c03181
ACS Omega 2024, 9, 28791−28805

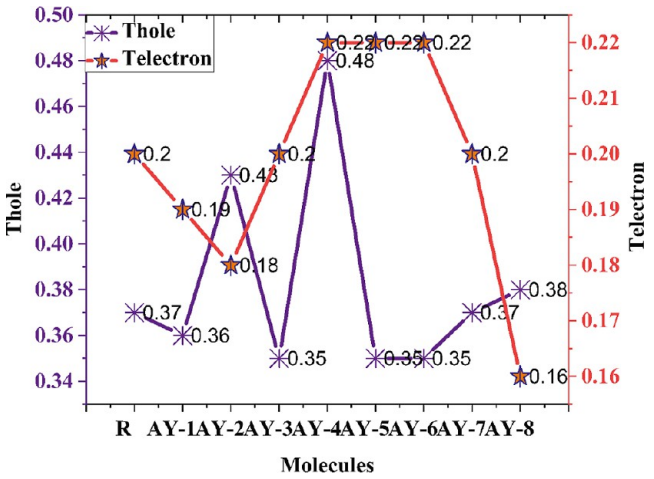

Figure 10. T_{hole} and $T_{electron}$ analysis of R and the designed AY1−AY8 molecules.

reorganization energies by introducing steric hindrance and electronic interactions. To clarify the electron reorganization energy of these NFAs, structural changes at cation and anion states with their respective torsional angles are as shown in Figures S6 and S7 (Supporting Information).

3.13. Fill Factor. When calculating the efficiency of a solar cell, the FF is one of the most important factors to consider. It measures how efficiently a solar cell converts light into electricity. A higher FF indicates that the solar cell is better at utilizing the available voltage and current to produce power, as shown in Table 4. A high FF suggests fewer losses in the cell due to recombination or resistive effects. It is calculated using eq 12.[45]

Table 4. Open-Circuit Voltage, FF, and PCE Comparison of R and All Designed Molecules

molecules	V_{oc}	FF %	PCE
R	1.76	90.45%	27.43%
AY-1	1.51	91.51%	23.40%
AY-2	1.36	90.76%	20.85%
AY-3	1.85	92.77%	29.03%
AY-4	1.91	92.94%	29.97%
AY-5	1.83	92.71%	28.72%
AY-6	1.81	92.64%	28.36%
AY-7	1.61	91.90%	24.93%
AY-8	1.63	91.99%	25.32%

$$FF = e^{\frac{V_{oc}}{K_{BT}}} - \frac{\ln\left(e^{\frac{V_{oc}}{K_{BT}}} + 0.72\right)}{eV_{oc}/K_{BT}} \quad (12)$$

J_{sc} represents the maximum current density a solar cell can generate when short-circuited under illumination. It measures a solar cell's efficiency. A higher J_{sc} indicates that the cell can generate more current, which is beneficial for increasing power output.

3.14. Open-Circuit Voltage. OSCs' open-circuit voltage (V_{oc}) is measured and analyzed to provide insights into their operating mechanism and performance assessment. Their open-circuit voltage often represents the total amount of current optical devices used. V_{oc} is measured at no voltage in solar technology. The photogenerated current and saturation voltage determine the solar device's open-circuit voltage. Both winds are crucial in solar devices' recombination processes. The total open-circuit voltage can only be measured using a set of scaling parameters.

The LUMO of the acceptor material is used as a measuring stick against the HOMO of the donor. Calculating the difference in energy between these two orbitals yields the value known as V_{oc}. Figure 11 shows that reducing the HOMO and increasing the LUMO of the donor material is required to attain large and high V_{oc} values. Many well-established donor materials have been recorded throughout history. Donor polymers like PTB7-Th are commonly employed because of their high visibility and low cost. Its HOMO energy level is −5.2 eV, and its LUMO energy level is −3.6 eV. Open-circuit voltages for all eight of our designed molecules (AY1−AY8) and the reference molecule (R) using the PTB7-Th donor polymer may be calculated using the following eq 13. In this calculation, we match the HOMO of the donor polymer with the LUMO of our newly constructed molecules to facilitate the most significant possible CT.[46]

$$V_{oc} = |E^{D}_{HOMO}| - |E^{A}_{LUMO}| - 0.3 \quad (13)$$

The reference molecule (R) has an open-circuit voltage of 1.76 V. Notably, the open-circuit voltages of all eight of our created molecules are within a narrow range of that of the reference molecule. The open-circuit voltages for AY1 through AY8 are 1.51, 1.36, 1.85, 1.91, 1.83, 1.81, 1.81, and 1.63 V, respectively. The designed molecules (AY1−AY8) all have relatively high open-circuit voltages, as shown by their values tabulated in Table 4, but AY3, AY4, AY5, and AY6 stand out. Their planar structure and the powerful withdrawing groups at their ends are likely responsible for this since they allow for efficient CT from the donor to acceptor. Each of the created molecules (AY1−AY8) has a different open-circuit voltage, with AY4 having the highest and AY1 having the lowest. Figure 11 shows, for the donor polymer PTB7-Th, the V_{oc} variation between the reference molecule (R) and all of the modified molecules (AY1 through AY8). From what has been said thus far, we may deduce that AY3, AY4, AY5, and AY6 have high V_{oc} values, indicating that they can conduct a lot of charge (43). As a result, every molecule is an excellent choice for making nonfullerene OSC devices.

3.15. Power Conversion Efficiency. PCE is a crucial parameter that quantifies the effectiveness of a solar cell in converting sunlight into electricity. It can be calculated as eq 14.[47]

$$PCE = \frac{J_{sc}V_{oc}FF}{P_{in}} \quad (14)$$

The photovoltaic characteristics of the reference R molecule were compared with the newly designed series (AY1-AY8). As shown in Figure 12, the calculated PCE values for the designed AY1-AY8 molecules are very close to the R molecule. Among these, the AY3-AY6 presented higher calculated PCE values than R, indicating our efficient molecular designing strategy. Moreover, the relevant calculated values of Voc, FF, and overall PCE are shown in Table 4. Furthermore, it is crucial to examine how the modification of the chemical structure of AY1−AY8 affects these characteristics in comparison to the reference molecule since this might provide light on how to fabricate better OSCs.

https://doi.org/10.1021/acsomega.4c03181
ACS Omega 2024, 9, 28791−28805

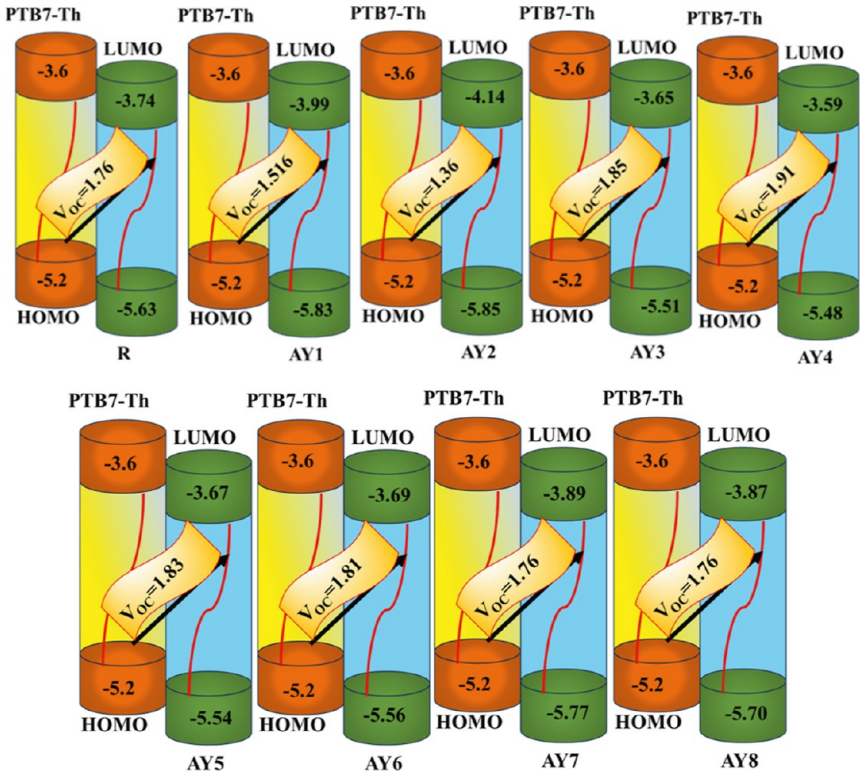

Figure 11. V_{oc} results of the reference R and the designed AY1−AY8 compounds.

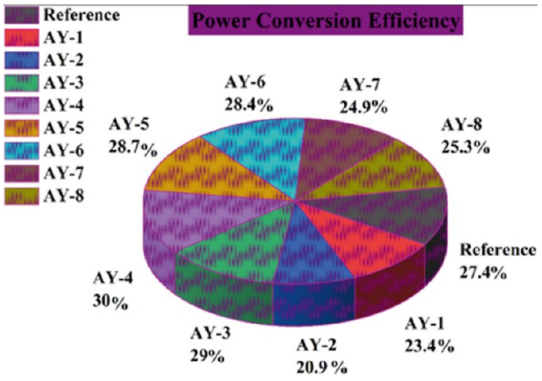

Figure 12. Estimated PCEs of R and the designed AY1−AY8 molecules.

3.16. CT Analysis. The assessment of charge transport dynamics between AY8 and the donor PTB7-Th is a pivotal aspect of our investigation, and it is meticulously conducted through the intricate analysis depicted in Figure 13a. This comprehensive study employs the computational approach of B3LYP/6-31G(d,p). AY8 is judiciously chosen as the acceptor molecule in our quest for complex formation for several compelling reasons. First, it boasts a notably narrow HOMO − LUMO energy gap, indicative of its exceptional charge-carrying capabilities. Additionally, AY8 exhibits low excitation and commendable reorganizational energy for hole and electron transport, further underscoring its suitability. Notably, it displays an acceptable open-circuit voltage and demonstrates a high red shift in its absorption spectrum, characteristics highly desirable for efficient solar cell applications. Meanwhile, PTB7-Th, a well-established and widely utilized donor, is selected as the ideal counterpart for complex formation in solar cell technology.

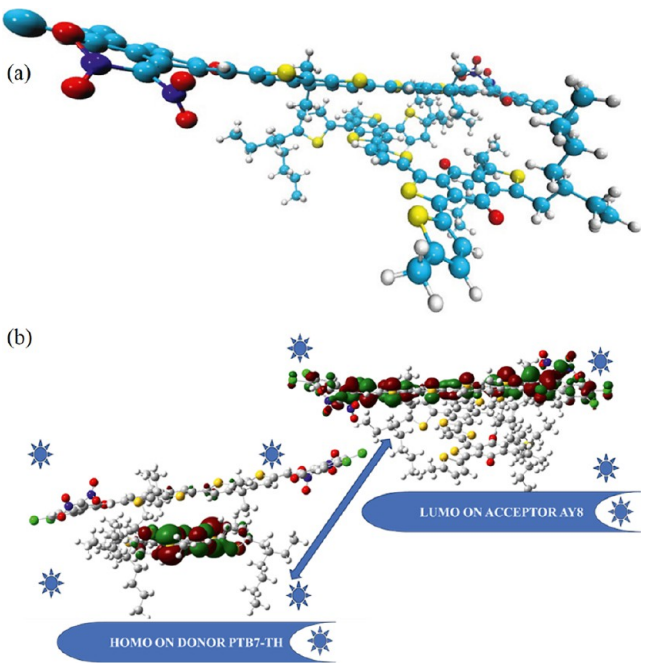

Figure 13. (a) Complex formation between AY8/PTB7-TH and (b) FMOs distribution between AY8 acceptor and PTB7-TH donor.

This intriguing distribution pattern, which serves as a cornerstone of our analysis, is corroborated independently through calculations performed at the MPW1PW91/6-31G-(d,p) level. As illustrated in Figure 13b, the charge density of the HOMO predominantly resides on the donor molecule, while the corresponding LUMO density predominantly localizes on the acceptor molecule, AY8. This compelling observation is concrete evidence of the charge mobility from

https://doi.org/10.1021/acsomega.4c03181
ACS Omega 2024, 9, 28791−28805

the donor to the acceptor molecule. Further substantiating our findings, the MO diagram presents robust evidence of electron mobility. It vividly portrays the impeccably aligned MOs between these two molecules, illustrating the seamless transfer of excited electrons from the HOMO to the LUMO. This harmonious molecular arrangement underscores the immense potential of our newly constructed materials, positioning them as up-and-coming acceptor candidates for the development of remarkably efficient OSCs.

4. CONCLUSIONS

In conclusion, our investigation has used quantum chemistry methods to probe the photovoltaic, photophysical, and electronic characteristics of a set of carefully constructed molecules designated AY1−AY8 along with R. We have proposed eight molecules (AY1−AY8) by making selective end-capping alterations on the scaffold of R. The developed molecules exhibit very low excitation energies and a HOMO − LUMO gap between 1.84 and 1.71 eV, in contrast to the R molecule (1.89 eV). Also, compared to the R molecule, the developed molecules exhibit good reorganizational energy for electrons (e = 0.0053 E_h) and holes (e = 0.4915−0.4566 E_h). This delicate balancing act of electrical characteristics makes them effective photovoltaic materials. Moreover, the improved red-shifted absorption seen for the designed AY1−AY8 series compared to that of the R molecule indicates our efficient designing strategy. The calculated absorption maxima are between 845.39 and 792.74 nm, and their lower excitation energies (E_x 1.52−1.47 eV) could contribute to their impressive photovoltaic and optoelectronic performances. Moreover, the open-circuit voltages of these designed molecules AY1−AY8 significantly improve in contrast to that of R due to their improved absorption and narrowing of the energy gap. Moreover, we see low binding energy values (E_b 0.14−0.02 eV), which makes them superior to the R molecule (E_b = 0.15 eV) in terms of the current−charge−density they provide. With its small band gap, strong charge mobility, significant dipole moment, low excitation and binding energies, and significant red shift in its absorption spectra, AY8 emerges as the good contender for fullerene-free OSCs among the array of created molecules AY1−AY8. All the proposed compounds AY1−AY8 had better photovoltaic qualities than the R molecule, indicating their efficacy as promising candidates for synthesis and fabricating efficient OSCs.

■ ASSOCIATED CONTENT

Data Availability Statement

The data presented in this study are provided in the Supporting Information.

Supporting Information

The Supporting Information is available free of charge at https://pubs.acs.org/doi/10.1021/acsomega.4c03181.

Employed end-capped structures; optimized structures of the designed materials; selection of the best DFT functional; LHE in solvent and gas phases; reorganization energy of molecules; torsional angle deviation cationic states; torsional angle deviation on anionic states; HOMO and LUMO energies and energy gap; percentage contribution of the donor and acceptor; oscillation strength and light harvesting energy in $CHCl_3$ and in the gas phase; UV−visible absorption, excitation energy, oscillating strength, and major MO assignments of R and designed AY1−AY8 molecules in the gas phase; and reorganizational energy of molecules (PDF)

■ AUTHOR INFORMATION

Corresponding Author

Riaz Hussain − *Department of Chemistry, University of Okara, Okara 56300, Pakistan*; orcid.org/0000-0003-4304-0451; Email: riazhussain@uo.edu.pk

Authors

Muzammil Hussain − *Department of Chemistry, University of Okara, Okara 56300, Pakistan*

Muhammad Adnan − *Graduate School of Energy Science and Technology, Chungnam National University, Daejeon 34134, Republic of Korea*; orcid.org/0000-0001-9224-3824

Zobia Irshad − *Graduate School of Energy Science and Technology, Chungnam National University, Daejeon 34134, Republic of Korea*; orcid.org/0000-0002-8130-4414

Hany W. Darwish − *Department of Pharmaceutical Chemistry, College of Pharmacy, King Saud University, Riyadh 11451, Saudi Arabia*

Complete contact information is available at: https://pubs.acs.org/10.1021/acsomega.4c03181

Author Contributions

‖M.H., M.A., and Z.I. contributed equally to this work.

Notes

The authors declare no competing financial interest.

■ ACKNOWLEDGMENTS

We thank COMSAT University Islamabad, Abbottabad Campus for providing their state-of-the-art computational facilities. The authors extend their appreciation to the Researchers Supporting Project number (RSPD2024R812), King Saud University, Riyadh, Saudi Arabia, for funding this work.

■ REFERENCES

(1) Yu, G.; Gao, J.; Hummelen, J. C.; Wudl, F.; Heeger, A. J. Polymer photovoltaic cells: enhanced efficiencies via a network of internal donor-acceptor heterojunctions. *Science* **1995**, *270* (5243), 1789−1791.

(2) Hoppe, H.; Sariciftci, N. S. Organic solar cells: An overview. *J. Mater. Res.* **2004**, *19* (7), 1924−1945.

(3) McGehee, M. D.; Topinka, M. A. Pictures from the blended zone. *Nat. Mater.* **2006**, *5* (9), 675−676.

(4) Lin, Y.; Wang, J.; Zhang, Z. G.; Bai, H.; Li, Y.; Zhu, D.; Zhan, X. An electron acceptor challenging fullerenes for efficient polymer solar cells. *Adv. Mater.* **2015**, *27* (7), 1170−1174.

(5) Li, Y. Molecular design of photovoltaic materials for polymer solar cells: toward suitable electronic energy levels and broad absorption. *Acc. Chem. Res.* **2012**, *45* (5), 723−733.

(6) Yao, H.; Cui, Y.; Yu, R.; Gao, B.; Zhang, H.; Hou, J. Design, synthesis, and photovoltaic characterization of a small molecular acceptor with an ultra-narrow band gap. *Angew. Chem., Int. Ed.* **2017**, *56* (11), 3045−3049.

(7) Cui, Y.; Yang, C.; Yao, H.; Zhu, J.; Wang, Y.; Jia, G.; Gao, F.; Hou, J. Efficient semitransparent organic solar cells with tunable color enabled by an ultralow-bandgap nonfullerene acceptor. *Adv. Mater.* **2017**, *29* (43), 1703080.

(8) Zhao, W.; Li, S.; Yao, H.; Zhang, S.; Zhang, Y.; Yang, B.; Hou, J. Molecular optimization enables over 13% efficiency in organic solar cells. *J. Am. Chem. Soc.* **2017**, *139* (21), 7148−7151.

(9) Xiao, Z.; Jia, X.; Li, D.; Wang, S.; Geng, X.; Liu, F.; Chen, J.; Yang, S.; Russell, T. P.; Ding, L. 26 mA cm- 2 Jsc from organic solar cells with a low-bandgap nonfullerene acceptor. *Sci. Bull.* **2017**, *62* (22), 1494−1496.
(10) Lin, Y.; Zhang, Z.-G.; Bai, H.; Wang, J.; Yao, Y.; Li, Y.; Zhu, D.; Zhan, X. High-performance fullerene-free polymer solar cells with 6.31% efficiency. *Energy Environ. Sci.* **2015**, *8* (2), 610−616.
(11) Adnan, M.; Mehboob, M. Y.; Hussain, R.; Irshad, Z. In silico designing of efficient C-shape non-fullerene acceptor molecules having quinoid structure with remarkable photovoltaic properties for high-performance organic solar cells. *Optik* **2021**, *241*, 166839.
(12) Adnan, M.; Irshad, Z.; Hussain, R.; Lee, W.; Yup Yang, J.; Lim, J. Influence of end-capped engineering on 3-dimenional star-shaped triphenylamine-based donor materials for efficient organic solar cells. *Arabian J. Chem.* **2023**, *16* (6), 104709.
(13) Adnan, M.; Irshad, Z.; Hussain, R.; Lee, W.; Kim, M.; Lim, J. Efficient ternary active layer materials for organic photovoltaics. *Sol. Energy* **2023**, *257*, 324−343.
(14) Safdar, S.; Adnan, M.; Hussain, R.; Yaqoob, J.; Khan, M. U.; Hussain, R.; Irshad, Z.; Alshehri, S. M. Role of 9-phenyl-9H-carbazole based hole transport materials for organic and perovskite photovoltaics. *Synth. Met.* **2023**, *297*, 117414.
(15) Wang, K.; Wei, H.; Li, Z.; Lu, S. Near-infrared small molecule acceptors based on 4H-cyclopenta [1, 2-b: 5, 4-b'] dithiophene units for organic solar cells. *Dyes Pigm.* **2021**, *196*, 109801.
(16) Dennington, R.; Keith, T.; Millam, J. *GaussView*. Version 5; Gaussian, Inc., 2009.
(17) Frisch, A. *Gaussian 09W Reference*; Gaussian, Inc.: Wallingford, USA, 2009; Vol: *470*; p 25.
(18) Civalleri, B.; Zicovich-Wilson, C. M.; Valenzano, L.; Ugliengo, P. B3LYP augmented with an empirical dispersion term (B3LYP-D*) as applied to molecular crystals. *CrystEngComm* **2008**, *10* (4), 405−410.
(19) Yanai, T.; Tew, D. P.; Handy, N. C. A new hybrid exchange-correlation functional using the Coulomb-attenuating method (CAM-B3LYP). *Chem. Phys. Lett.* **2004**, *393* (1−3), 51−57.
(20) Adamo, C.; Barone, V. Exchange functionals with improved long-range behavior and adiabatic connection methods without adjustable parameters: The m PW and m PW1PW models. *J. Chem. Phys.* **1998**, *108* (2), 664−675.
(21) Yan, C.; Barlow, S.; Wang, Z.; Yan, H.; Jen, A. K. Y.; Marder, S. R.; Zhan, X. Non-fullerene acceptors for organic solar cells. *Nat. Rev. Mater.* **2018**, *3* (3), 18003.
(22) May, R. A.; Stevenson, K. J. *Software Review of Origin 8*; ACS Publications, 2009.
(23) Naveed, A.; Khera, R. A.; Azeem, U.; Zubair, I.; Farhat, A.; Ayub, A. R.; Iqbal, J. Tuning the optoelectronic properties of benzodithiophene based donor materials and their photovoltaic applications. *Mater. Sci. Semicond. Process.* **2022**, *137*, 106150.
(24) Lu, T.; Chen, F. Multiwfn: A multifunctional wavefunction analyzer. *J. Comput. Chem.* **2012**, *33* (5), 580−592.
(25) Adnan, M.; Lee, J. K. Highly efficient planar heterojunction perovskite solar cells with sequentially dip-coated deposited perovskite layers from a non-halide aqueous lead precursor. *RSC Adv.* **2020**, *10* (9), 5454−5461.
(26) Siddique, S. A.; Altaf, S.; Ahmed, E.; Naveed, S.; Siddique, M. B. A.; Hussain, R.; Liu, X.; Rauf, A.; Arshad, M. Discovery of versatile bat-shaped acceptor materials for high-performance organic solar cells-a DFT approach. *Int. J. Energy Res.* **2022**, *46* (10), 13393−13408.
(27) Adnan, M.; Lee, J. k. All Sequential Dip-Coating Processed Perovskite Layers from an Aqueous Lead Precursor for High Efficiency Perovskite Solar Cells. *Sci. Rep.* **2018**, *8*, 2168.
(28) Siddique, S. A.; Siddique, M. B. A.; Hussain, R.; Liu, X.; Mehboob, M. Y.; Irshad, Z.; Adnan, M. Efficient tuning of triphenylamine-based donor materials for high-efficiency organic solar cells. *Comput. Theor. Chem.* **2020**, *1191*, 113045.
(29) Lu, C.; Paramasivam, M.; Park, K.; Kim, C. H.; Kim, H. K. Phenothiazine functionalized multifunctional A- π-D- π-D- π-A-type hole-transporting materials via sequential C-H arylation approach for efficient and stable perovskite solar cells. *ACS Appl. Mater. Interfaces* **2019**, *11* (15), 14011−14022.
(30) Paramasivam, M.; Chitumalla, R. K.; Singh, S. P.; Islam, A.; Han, L.; Jayathirtha Rao, V.; Bhanuprakash, K. Tuning the photovoltaic performance of benzocarbazole-based sensitizers for dye-sensitized solar cells: a joint experimental and theoretical study of the influence of π-spacers. *J. Phys. Chem. C* **2015**, *119* (30), 17053−17064.
(31) Paramasivam, M.; Chitumalla, R. K.; Jang, J.; Youk, J. H. The impact of heteroatom substitution on cross-conjugation and its effect on the photovoltaic performance of DSSCs-a computational investigation of linear vs. cross-conjugated anchoring units. *Phys. Chem. Chem. Phys.* **2018**, *20* (35), 22660−22673.
(32) Mahalingavelar, P. How end-capped acceptors regulate the photovoltaic performance of the organic solar cells: a detailed density functional exploration of their impact on the A-d- π-D-A type small molecular electron donors. *Energy Fuels* **2022**, *36* (4), 2095−2107.
(33) Kanai, K.; Akaike, K.; Koyasu, K.; Sakai, K.; Nishi, T.; Kamizuru, Y.; Nishi, T.; Ouchi, Y.; Seki, K. Determination of electron affinity of electron accepting molecules. *Appl. Phys. A: Mater. Sci. Process.* **2009**, *95*, 309−313.
(34) Brus, L. E. A simple model for the ionization potential, electron affinity, and aqueous redox potentials of small semiconductor crystallites. *J. Chem. Phys.* **1983**, *79* (11), 5566−5571.
(35) Pal, S.; Roy, R.; Chandra, A. K. Change of hardness and chemical potential in chemical binding: a quantitative model. *J. Phys. Chem.* **1994**, *98* (9), 2314−2317.
(36) Senet, P. Chemical hardnesses of atoms and molecules from frontier orbitals. *Chem. Phys. Lett.* **1997**, *275* (5−6), 527−532.
(37) Chermette, H. Chemical reactivity indexes in density functional theory. *J. Comput. Chem.* **1999**, *20* (1), 129−154.
(38) Hussain, R.; Khan, M. U.; Mehboob, M. Y.; Khalid, M.; Iqbal, J.; Ayub, K.; Adnan, M.; Ahmed, M.; Atiq, K.; Mahmood, K. Enhancement in photovoltaic properties of N, N-diethylaniline based donor materials by bridging core modifications for efficient solar cells. *ChemistrySelect* **2020**, *5* (17), 5022−5034.
(39) Wang, J.; Zhan, X. Fused-ring electron acceptors for photovoltaics and beyond. *Acc. Chem. Res.* **2021**, *54* (1), 132−143.
(40) Adnan, M.; Kim, H. S.; Jeong, H.; Ko, H. M.; Woo, S. K.; Lee, J. K. Efficient synthesis and characterization of solvatochromic fluorophore. *Bull. Korean Chem. Soc.* **2017**, *38* (9), 1052−1057.
(41) Lyakurwa, M.; Numbury, S. B. DFT and TD-DFT study of Optical and Electronic Properties of new donor-acceptor-donor (D-A-D′) monomers for polymer solar cells. *Oxford Open Mater. Sci.* **2023**, *3* (1), itad003.
(42) Irshad, Z.; Adnan, M.; Lee, J. K. Controlling phase and morphology of all-dip-coating processed HC (NH2) 2PbI3 perovskite layers from an aqueous halide-free lead precursor. *J. Phys. Chem. Solids* **2022**, *160*, 110374.
(43) Adnan, M.; Iqbal, J.; BiBi, S.; Hussain, R.; Akhtar, M. N.; Rashid, M. A.; Eliasson, B.; Ayub, K. Fine tuning the optoelectronic properties of triphenylamine based donor molecules for organic solar cells. *Z. Phys. Chem.* **2017**, *231* (6), 1127−1139.
(44) Sivakumar, G.; Paramasivam, M.; Bharath, D.; Rao, V. J. Energy level tuning of 'Z'-shaped small molecular non-fullerene electron acceptors based on a dipyrrolo [2, 3-b: 2′, 3′-e] pyrazine-2, 6 (1 H, 5 H)-dione acceptor unit for organic photovoltaic applications: A joint experimental and DFT investigation on the effect of fluorination. *New J. Chem.* **2019**, *43* (13), 5173−5186.
(45) Marcus, R. A. Chemical and electrochemical electron-transfer theory. *Annu. Rev. Phys. Chem.* **1964**, *15* (1), 155−196.
(46) Hossain, M. K.; Toki, G. F. I.; Alam, I.; Pandey, R.; Samajdar, D. P.; Rahman, M. F.; Islam, M. R.; Rubel, M. H. K.; Bencherif, H.; Madan, J.; et al. Numerical simulation and optimization of a CsPbI 3-based perovskite solar cell to enhance the power conversion efficiency. *New J. Chem.* **2023**, *47* (10), 4801−4817.
(47) Zhang, L.; Shen, W.; He, R.; Liu, X.; Tang, X.; Yang, Y.; Li, M. Fine structural tuning of diketopyrrolopyrrole-cored donor materials

https://doi.org/10.1021/acsomega.4c03181
ACS Omega 2024, 9, 28791−28805

for small molecule-fullerene organic solar cells: A theoretical study. *Org. Electron.* **2016**, *32*, 134−144.

https://doi.org/10.1021/acsomega.4c03181
ACS Omega 2024, 9, 28791−28805